Eurasian Chemico-Technological Journal 16 (2014) 27-34

Fabrication of Yttrium Ferrite Nanoparticles by Solution Combustion Synthesis

A.A. Saukhimov[1,2], M.A. Hobosyan[1], G.C. Dannangoda[1],
N.N. Zhumabekova[2], S.E Kumekov[2] and K.S. Martirosyan[1*]

[1]University of Texas, Brownsville, 80 Fort Brown, Brownsville, Texas 78520, USA
[2]Kazakh National Technical University after K.I. Satpaev, Satpaev st. 22, 050013 Almaty, Kazakhstan

Abstract

The ternary oxide system Y-Fe-O presents fascinating magnetic properties that are sensitive to the crystalline size of particles. There is a major challenge to fabricate these materials in nano-crystalline forms due to particle conglomeration during nucleation and synthesis. In this paper we report the fabrication of nano sized crystalline yttrium ferrite by solution combustion synthesis (SCS) where yttrium and iron nitrates were used as metal precursors with glycine as a fuel. The magnetic properties of the product can be selectively controlled by adjusting the ratio of glycine to metal nitrates. Yttrium ferrite nano-powder was obtained by using three concentration of glycine (3, 6 and 10 wt.%) in the initial exothermic mixture. Increasing glycine content was found to increase the reaction temperature of the system. The structural and magnetic properties of yttrium ferrite before and after annealing at temperature of 1000 °C were investigated by X-ray diffractometry, Differential Scanning Calorimetry (DSC) and cryogenic magnetometry (PPMS, Quantum Design). X-ray diffraction showed that, a broad diffraction peak was found for all samples indicating the amorphous nature of the product. Particle size and product morphology analysis identified that, Nitrate/glycine combustion caused considerable gas evolution, mainly carbon dioxide, N_2 and H_2O vapor, which caused the synthesized powders to become friable and loosely agglomerated for glycine concentration from 3 wt.% up to 10 wt.%. The study of the magnetic properties of produced materials in a metastable state was performed by measuring dependencies of Magnetization (M) on temperature, and magnetization on magnetic field strength between 5 K and 300 K. Magnetization measurements on temperature zero-field-cooled and field-cooled show different patterns when the fraction of glycine is increased. The analysis of zero-field-cooled (ZFC), field-cooled (FC) and magnetization curves of annealed samples confirmed that nanoparticles exhibit superparamagnetic behavior. The increasing concentration of glycine leads to an increased blocking temperature.

Keywords: Yttrium ferrite, solution combustion synthesis, nanoparticles, superparamagnetic, blocking temperature.

Introduction

Yttrium ferrites are complex oxide compounds that exhibit soft magnetic properties that can be used in electronic devices for high frequency applications [1, 2]. Yttrium is considered a rare earth element since it tends to occur in ore deposits along with lanthanides and exhibits similar physical and chemical properties. Recent studies also demonstrate that yttrium ferrite displays electrical and magnetic coupling which shows ferroelectricity near the ferrimagnetic transition temperature around 250 K [3]. Rare-earth ferrites are often prepared from high temperature solid-state reactions of the corresponding simple oxides [4]. However, this process suffers from: excessive particle growth, irregular stoichiometries, and formation of undesirable phases. Other synthesis routes have also been proposed including chemical precipitation [5, 6], thermal decomposition [7], solvothermal treatment [8], sonochemical approaches [9] and combustion synthesis [10, 11].

Solution combustion synthesis (SCS) is a simple and rapid chemical processing technique suitable for producing a variety of nano size materials (<100 nm) [12-14]. The process involves using an aqueous solution of different oxidizers (metal nitrates) and fuels (e.g. glycine, urea, hexamethylene tetra amine (HMTA) or hydrazine). Various oxides structures

* Corresponding author. E-mail: Karen.Martirosyan@utb.edu

have been prepared via solution combustion such as perovskites (e.g. $LaFeO_3$), spinels (e.g. $MgAl_2O_4$), garnets (e.g. $Y_3Al_5O_{12}$), hexaferrites (e.g. $SrFe_{12}O_{19}$), etc. Solution combustion synthesis is an attractive approach to synthesize nanomaterials for a variety of applications, including electronics, catalysis and biotechnology [13].

For this study, three different concentrations of glycine (3, 6 and 10 wt.%) were used in the initial exothermic mixture to produce nanostructured yttrium ferrite. Structural and magnetic properties of nanocrystalline products were characterized by thermogravimetric and differential scanning calorimetry (TG/DSC) and cryogenic magnetometry (Physical Property Measurement System, PPMS, Quantum Design).

Experimental

High purity Yttrium nitrate pentahydrate (99.9%) and Iron (III) nitrate nonahydrate (98%) were used as oxidizers and organic compound amino acid (glycine, $CH_2NH_2CO_2H$) was used as the fuel to prepare yttrium ferrite nanoparticles via solution (nitrate–glycine) combustion synthesis. The chemicals were purchased from Sigma-Aldridge Co and used without any purification. In conventional solution combustion synthesis both fuel and oxidizer are dissolved in water to form a homogeneous solution.

The reagents $Y(NO_3)_3{\cdot}5H_20$, $Fe(NO_3)_3{\cdot}9H_20$ and glycine were added to 3 ml distilled water in a beaker and stirred for one hour. In accordance with the SCS method, the aqueous solution was heated on a hotplate to slowly evaporate the water away. During the final stages of evaporation, boiling, frothing, smoldering, flaming and fumes were observed, resulting in complex nanocrystallites of yttrium oxide. The local combustion temperature (T_c) inside the reactant mixture was measured by an S-type (Pt-Rh) thermocouple, 0.1 mm diameter and inserted in the center of sample. Thermocouple readings were recorded and processed by an Omega data acquisition board connected to a computer. Differential scanning calorimetry (DSC) of the mixtures were used to identify phase transitions and chemical reactions that occured under an air atmosphere in the temperature range of 20-1000 °C with a 20 °C/min heating rate. To increase crystallinity of the powder and enhance the desired magnetic properties the synthesized products were annealed for 1 h in air at 1000 °C.

The composition and crystal structure of the products were determined by X-ray diffraction (Siemens D5000 diffractometer) with Cu K_R radiation (1.54056 Å). Scans were taken at room temperature over $5° < 2\Theta < 80°$ at 0.05° intervals. Particle morphology and electron microprobe analysis were determined by scanning electron microscopy (SEM; JEOL JAX8600, Japan) of powders fixed to a graphite disk. A Coulter SA 3100 BET analyzer was used to measure particle size and surface area distributions.

Magnetic properties of samples were determined by vibrating sample magnetometer (Quantum Design, Physical Property Measurement System). Saturation (M_s), remanant magnetization (M_r) and coercivity (H_c) were estimated from the hysteresis loops obtained at 300 K and 5 K under a maximum applied field of ±90 kOe. Zero-field-cooled (ZFC) and field-cooled (FC) magnetization curves were measured from 1.9-300 K using a 100 Oe field.

Results and Discussion

The ratio between the oxidizer (yttrium and iron nitrates) and fuel (glycine) in the molten solution had a strong impact on the temperature rise, reaction period and particle size. In addition, adjusting the ratio of glycine to metal nitrates allowed the combustion temperature to be tuned and controlled. Lower concentrations of glycine were found to generate lower temperatures that may lead to metastable phase products with smaller particle size. To conduct safe and controlled combustion reactions, mixtures with less than 10 g of metal nitrates/glycine were used. Observations of reaction performance for the three different glycine concentrations during combustion synthesis are presented in Table 1.

Table 1
Reaction behavior and associated reaction temperature during solution combustion synthesis

Characterization of process	3 wt.% gly	6 wt.% gly	10 wt.% gly
Boiling temperature °C	123	132	135
Vaporization temperature, °C	162	174	185
Decomposition temperature °C	193	208	214
Brown vapor generation, °C	238	250	268
Reaction completed, °C	257	279	300

DSC Analysis

Liquefied yttrium, iron nitrates and glycine formed a clear homogeneous solution after mixing. The mixture boiled, frothed, and then ignited, releasing large amounts of gases and produced brown nanoparticles. Thermo gravimetric and differential scanning calorimeter analysis was performed to

study the behavior of nano crystalline powders obtained using 3, 6 and 10 wt.% of glycine. The DSC curves are shown in Fig. 1. According to DSC data, the main weight decrease occurs at about 500 °C: for 3 wt.% gly – 27.82% (total 29.48%), 6 wt.% gly – 22.23% (total 24.3 %) and 10 wt.% gly – 10.73% (total 15.91%). The observed weight decrease was attributed to incomplete combustion reactions during synthesis. Therefore, for the sample with 10 wt.% glycine, the combustion reaction was observed to be more complete. For the first two samples, the heat curves show two endotherm peaks, the first peak (120 J/g and 39 J/g for mixtures containing 3 wt.% and 6 wt.% glycine, respectively) corresponding to evaporation of remnant water, and the second (90 J/g and 56 J/g, respectively) to the final decomposition of any remnant nitrates. At 780 °C for both samples we observe an exothermic peak without change of any weight change, which is indicates a phase transformation. The phase transformation is irreversible, since after cooling the sample and reheating it there is no characteristic exothermic peak. For the third sample with 10 wt.% glycine, initially we don't observe an endotherm peak demonstrating that the conversion of the product was significantly more complete (less moisture and nitrate remains after the combustion) than the other two samples. Additionally, a small weight decrease is observable prior to phase transformation, 2% for 770 °C which is absent in the other samples. We attribute this feature to excess glycine trapped in the powder that eventually reacts with air. Thus, greater amount of glycine are increase the decomposition rate. DSC results clearly demonstrate the effectiveness of the self-propagating combustion for the preparation of pure phase nanocrystalline particles.

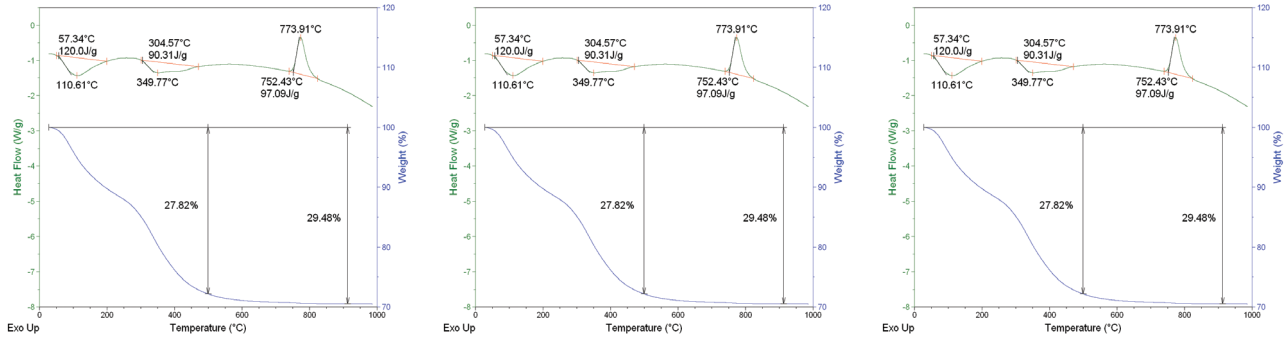

Fig. 1. Differential scanning calorimetric analysis of the system at 3, 6 and 10 wt.% of glycine.

Crystal Structure, Composition and XRD Analysis

Figure 2 shows X-ray diffraction pattern of as-synthesized yttrium ferrite at three different concentration of glycine. A broad diffraction peak was found for all samples indicating the amorphous nature of the product. After annealing at 1000 °C diffraction patterns (Fig. 3) indicate high intensity reflection confirming the presence of single phase of $Y_3Fe_5O_{12}$ with a garnet structure (standard database JCPDS, 33-363). The crystallite size of yttrium ferrites nanoparticles was calculated using the Scherrer equation [15] based on X-ray diffraction line broadening:

$$d = \frac{B\lambda}{\beta \cos\theta} \qquad (1)$$

where d is the average crystallite size of the phase under investigation, B is the Scherrer constant (0.89), λ is the wavelength of X-ray beam used, β is the full width at half maximum (FWHM) of the diffraction peak and θ is the Bragg's angle. Crystallite sizes were calculated to be 24.47 and 72 nm for powders obtained with 3, 6 and 10 wt.%, glycine respectively, followed by annealing at 1000 ºC. Thus, the crystallite size of yttrium ferrite was larger at elevated glycine concentration and consequently higher combustion temperatures.

Table 2 shows energy-dispertive X-ray spectroscopy (EDX) analysis of $Y_3Fe_5O_{12}$ annealed at 1000°C which differ slightly from the theoretical values for yttrium iron garnet (YIG which is referred for atomic percent of Y, Fe and O as 15%, 25% and 60%, respectively). The difference could be due to the nature of EDX mapping which does not necessarily represent the bulk composition of the entire sample. Table 2 confirms there are no impurities for the YIG samples due to high purity starting materials and stringent control of preparation procedures. Atomic concentrations are dominated by oxygen followed by iron then yttrium. The atomic percent of iron to oxygen is a constant and compared to oxygen, the higher peak of oxygen in the spectrum indicated higher concentration of oxygen comparing to the iron element.

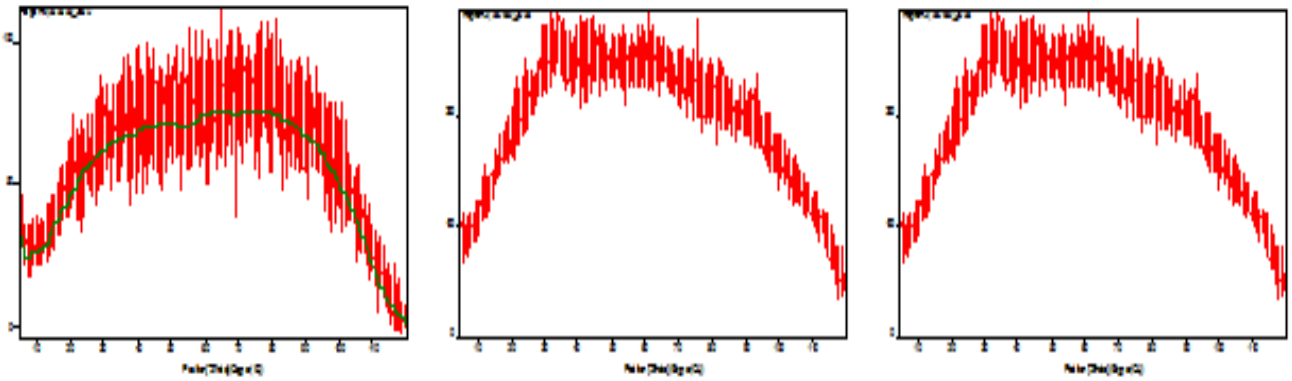

2θ (degree) 2θ (degree) 2θ (degree)

Fig. 2. X-ray diffraction pattern of as-synthesized yttrium ferrite at three different concentration of glycine.

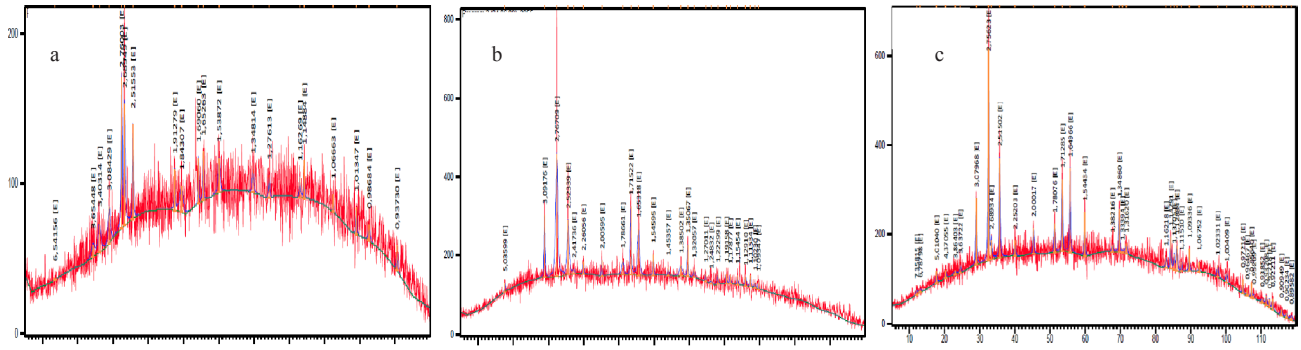

Fig. 3. XRD patterns of yttrium ferrites powder produced at different glycine concentrations (a) – 3 wt.%; (b) – 6 wt.% and (c) – 10 wt.% and annealed at 1000 °C.

Table 2
Elemental composition (weight % and atomic %) of $Y_3Fe_5O_{12}$ samples obtained with 3-10 wt.% glycine concentration and annealed at 1000 °C determined by EDX analysis.

Glycine concentration, (wt.%)	$Y_3Fe_5O_{12}$ Sample	Yttrium (Y)	Iron (Fe)	Oxygen (O)
3	Weight %	34.42	30.63	34.95
	Atomic %	15.20	21.69	63.11
6	Weight %	35.64	31.56	32.80
	Atomic %	16.04	20.54	63.42
10	Weight %	37.81	32.92	29.27
	Atomic %	15.53	20.24	64.23

Particle Size and Product Morphology

Nitrate/glycine combustion caused considerable gas evolution, mainly carbon dioxide, N_2 and H_2O vapor, which caused the synthesized powders to become friable and loosely agglomerated. Particle size distribution and the particles surface area were determined by a Coulter SA 3100 Brunauer-Emmett-Teller (BET) analyzer. BET analysis of as-synthesized yttrium ferrite particles confirms that for increasing glycine concentration from 3 wt.% up to 10 wt.% the specific surface area of product decreases monotonically from 42.1 m^2/g to 18.2 m^2/g. Thus, decreasing the fuel concentration decreases the maximum combustion temperature and increases particles surface area.

By using BET measured specific surface area of the powder we can estimate the product average particle size. The specific surface area (S) of a non-porous spherical particle is inversely proportional to its diameter (D), i.e.,

$$D = \frac{6}{\rho \cdot S} \qquad (2)$$

where S – [m^2/g], ρ is the theoretical density, [g/m^3]. Experiments determined S to be varied from 18.2–42.1 m^2/g. Assuming that the as-synthesized yttrium ferrite particles are spherical with density $\rho = 5.17$ g/cm^3, their size is predicted to be ~ 27 nm at (3 wt.%) and ~ 64 nm (10 wt.%). The particles morphology of as-synthesized yttrium ferrite prepared with three different concentrations of glycine 3, 6 and 10 wt.% is shown in Fig. 4. Higher magnification of the products shows that the agglomerates contained 30–80 nm particles with smooth surfaces. Solution

combustion synthesis caused considerable gas evolution generating many pores so that the as-synthesized powders became homogeneously agglomerated. All combustion products were friable, and had a spongy porous structure with porosity of up to 80%. Concentration of residual carbon was lower than 1 wt.%.

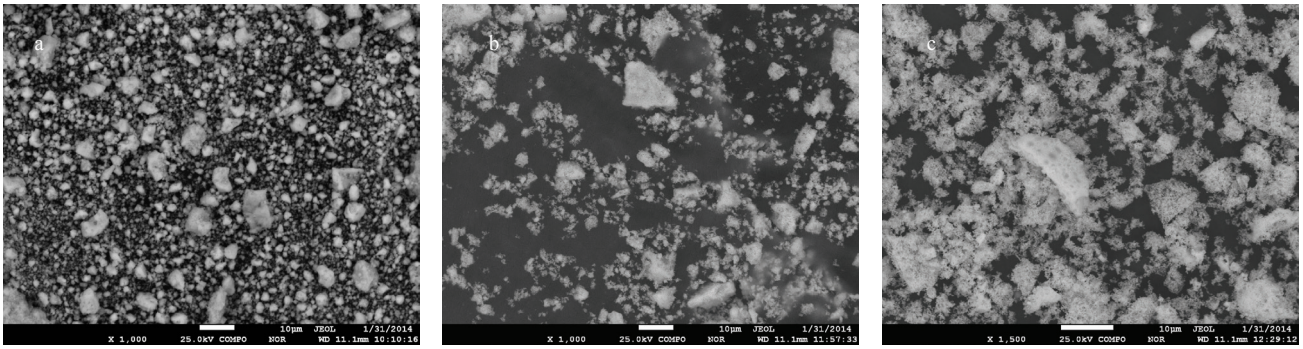

Fig. 4. SEM images of yttrium ferrites powder produced at different glycine concentrations (a) – 3 wt.%; (b) – 6 wt.% and (c) – 10 wt.% and annealed at 1000 °C.

Magnetic Properties of Yttrium Ferrite

The study of the magnetic properties of produced materials in a metastable state was performed by measuring dependencies of Magnetization (M) on temperature, and magnetization on magnetic field strength between 5 K and 300 K. Magnetization measurements on temperature zero-field-cooled and field-cooled show different patterns when the fraction of glycine is increased (Fig. 5). Difference between ZFC and FC curves may indicate superparamagnetic behaviour of nanoparticles. As is commonly understood, magnetic moments of superparamagnetic particles are chaotically oriented in a matrix in the absence of a magnetic field, and the total magnetic moment of the sample equals zero. When cooling in the absence of a magnetic field, particle moments are "frozen" at a certain blocking temperature (T_b), meanwhile their distribution in a matrix remains chaotic, and the total moment equals zero as before. Blocking temperature T_b depends on the volume of the particles and their anisotropy. If the anisotropy stays the same, T_b depends only on the volume, the bigger the particle volume the higher the blocking temperature. The blocking temperature is directly connected with the size of the particles by the formula:

$$T_b = \frac{KV}{25 K_B} \tag{3}$$

where K – magnetic anisotropy constant; V – volume of the particle; k_B – Boltzmann constant. According to Fig. 6, the average blocking temperature for the three samples is determined in the following order: $T_b = 25$ K, $T_b = 40$ K, $T_b = 70$ K. According to the formula it can be concluded that the samples with 3 wt.% glycine have the smallest particle size.

Experimentally the blocking temperature, above which the particles move to a ferromagnetic state, is determined at the point where FC and ZFC curves diverge. In the case of monosized particles this will coincide with the maximum on ZFC curve. In the case of dispersion of a distribution of particle sizes, the maximum temperature on ZFC curves (T_b – blocking temperature) will differ by the temperature at which divergence of FC and ZFC curves occurs (T_i – irreversible temperature).

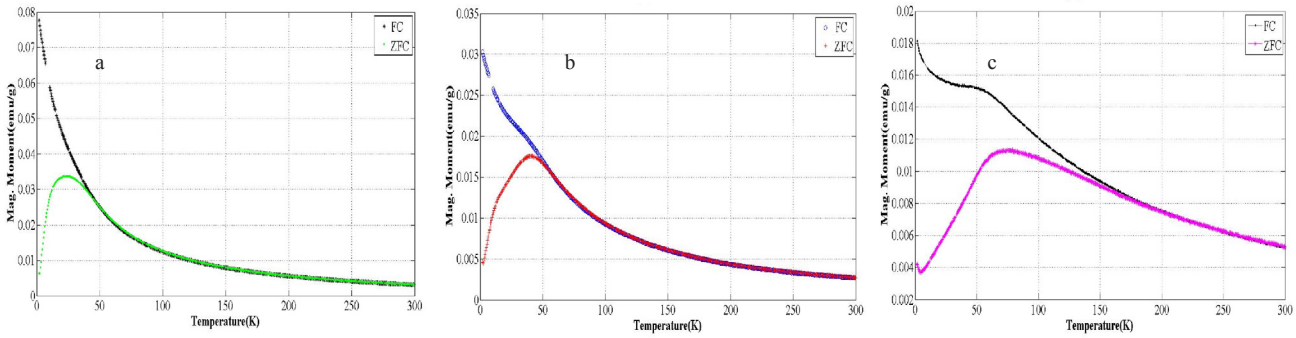

Fig. 5. Zero-field-cooled (ZFC) and field-cooled (FC) curves for samples of as synthesized yttrium ferrite produced at different glycine concentrations (a) – 3 wt.%, (b) – 6 wt.% and (c) – 10 wt.% before annealing.

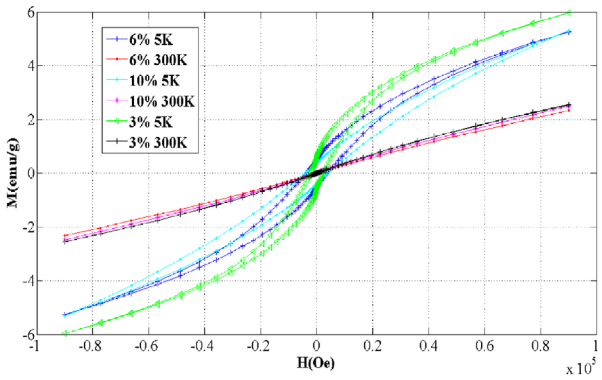

Fig. 6. Magnetic hysteresis of yttrium ferrites for different glycine concentrations at 5 K and 300 K before annealing.

Irreversible temperatures and magnetizations at these points for three diagrams have the following values: 3 wt.% T_i = 40 K, M = 0.03 emu/g; 6 wt.% T_i = 44 K, M = 0.017 emu/g; 10 wt.% T_i = 170 K, M = 0.008 emu/g. In a given sample differences between temperature values T_b and T_i appear, which may be related to a wide distribution of particles by size. In Fig. 6 it can be seen that increasing glycine content influences the blocking temperature for different samples. As temperature increases, magnetization of the system increases due to large particles begin moving to an unblocked state. Thus, particles size distribution explain why magnetization of the system increases gradually with increasing temperature in an external magnetic field.

In further investigations we analyzed the magnetisation M versus magnetic field strength (H) for three yttrium ferrite samples (Fig. 6) obtained directly after combustion synthesis. Dependencies of magnetization by the applied magnetic field strength were measured at temperatures of 5 K and 300 K corresponding to temperatures below and above the blocking temperatures. The results are presented in Table 3 and confirm that $Y_3Fe_5O_{12}$ synthesized by different glycine concentrations exhibits weak saturation and remnant magnetization.

Table 3

Characterization of hysteresis loop for yttrium ferrite samples before annealing at 1000 °C

Characteristics	3 wt.% gly		6 wt.% gly		10 wt.% gly	
	5 K	300 K	5 K	300 K	5 K	300 K
Saturation magnetization, (emu/g)	5.96	2.5582	5.253	2.319	5.3	2.486
Remnant magnetization, (emu/g)	0.57	0.00061	0.478	0.00043	0.35	0.00116
Coercivity force, (Oe)	2370	15.90	3844	15.00	4018	16.7

Data indicated that the largest saturation and remnant magnetization occurs in the $Y_3Fe_5O_{12}$ sample synthesized with 3 wt.% glycine, while the 10 wt.% glycine sample exhibited the largest coercivity.

Results of the analysis show that magnetization curves for the three $Y_3Fe_5O_{12}$ samples at temperatures of 5 K and 300 K are distinctly different. The hysteresis plot for samples $Y_3Fe_5O_{12}$ at 300 K shows a linear increase with field, with no sign of saturation up to 9000 Oe, resembling a paramagnet. The $Y_3Fe_5O_{12}$ samples at 5 K never reaches saturation at a magnetic field of 9000 Oe. This indicates that sample at 5 K is a weak ferromagnetic, as in the case of orthoferrite. Large values of the coercive force at 5 K coincide with the rise of magnetic anisotropy, which prevents the alignment of moments along the direction of applied field. For all three samples we observe a decline in the magnetization with increased glycine. This occurrence can be explained by decline of growth of some domains through decrease of others and shift of boundaries between them. Increased glycine content exhibited an increased coercive force. Hysteresis loops exhibit an energy loss due to the magnetization which can be calculated by the relation:

$$W = \int HdB \qquad (4)$$

The lowest value of loss corresponding to the formula (4), occurs in the sample with 3 wt.% glycine.

Similar magnetic measurements (shown in Figs. 7 and 8) performed for the three samples after annealing at 1000 °C. Investigations for samples after annealing show that the divergence of ZFC and FC curves occurs at the following values of T_i: 3 wt.% T_i = 290 K, 6 wt.% T_i = 275 K, 10 wt.% T_i = 280 K. Figure 8 shows distinct differences in the magnetization versus temperature curve for ZFC measurements in all three samples. The blocking temperature T_b for yttrium ferrites with 3 wt.% glycine is 255 K, 6 wt.% glycine samples have three values of

T_b – 70 K, 140 K, and 260 K; 10 wt.% has two values of T_b – 70 K and 270 K. As the temperature rises, the magnetization of the system increases due to large particles moving from a blocked to unblocked state. After reaching T_b the magnetization begins to relax and declines with increasing temperature. Furtherm ore, repeated activation of magnetic particles at temperatures above 250 K is observed. The largest magnetic contribution is made by particles that comprise the major volume fraction. Thus, analysis of ZFC and FC curves before and after annealing at 1000 °C shows a dramatic increase of yttrium ferrite particles and a corresponding rise in the transition temperature to a ferrimagnetic state.

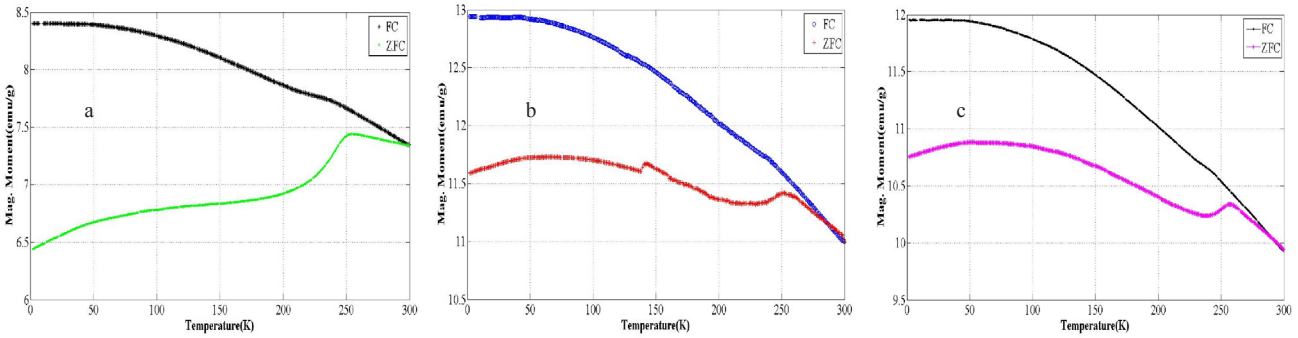

Fig. 7. Zero-field-cooled (ZFC) and field-cooled (FC) curves for samples of yttrium ferrite at different glycine concentrations at (a) – 3 wt.%, (b) – 6 wt.% and (c) – 10 wt.% after annealing at 1000 °C.

Similarly, M versus H measurements (Fig. 8) were conducted for the $Y_3Fe_5O_{12}$ samples after annealing at 1000 °C. Hysteresis curves measured after annealing show a rectangular shape which corresponds to the soft magnetic materials. Results of magnetic measurements are summarized in Table 4.

After annealing, changes in domain structure has been observed in the yttrium ferrite samples, so that the easy axis coincides with the direction of the applied field H and the magnetization occurs through the domain wall motion. Magnetization curves of $Y_3Fe_5O_{12}$ after annealing show that coercive forces decreased significantly while saturation magnetization increased in several orders.

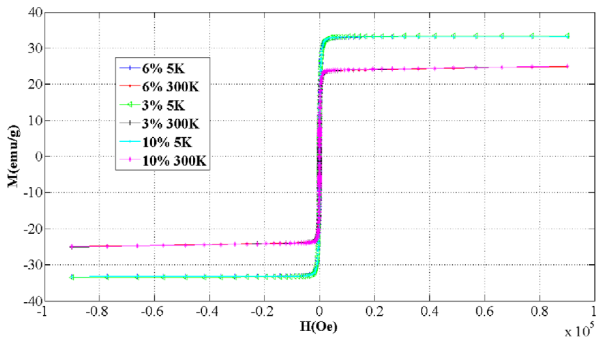

Fig. 8. Magnetic hysteresis loop of yttrium ferrite at different glycine concentrations under 5 K and 300 K after annealing at 1000 °C.

Table 4

Characterization of hysteresis loops for samples $Y_3Fe_5O_{12}$ samples after annealing to 1000 °C

Characteristics	3 wt.% gly		6 wt.% gly		10 wt.% gly	
	5 K	300 K	5 K	300 K	5 K	300 K
Saturation magnetization-M_s (emu/g)	33.52	25	33.24	24.91	33.20	24.96
Remnant magnetization-M_r (emu/g)	4.18	1.80	6.69	3.87	8.72	6.08
Coercivity force (Oe)	45.80	8.51	63.70	35.40	84.10	57.30
Squareness ratio (M_r/M_s)	0.12	0.07	0.20	0.16	0.26	0.24

The increase of the blocking temperatures after annealing for all three compositions was due to the increasing of particle size of yttrium ferrites. We observed a rise in magnetic susceptibility (μ) for $Y_3Fe_5O_{12}$ and a sharp shift in domain boundaries specified by increasing the sizes of domains due to an increase in the resultant magnetic moment in conditions of decreasing sizes of neighboring domains.

Conclusions

The experiments demonstrate the feasibility of direct preparation of highly nano crystalline yttrium ferrite nanoparticles by solution combustion synthesis. The enhancement of interaction of particles between yttrium nitrate pentahydrate and iron (III) nitrate nonahydrate with 10 wt.% glycine is confirmed by DSC curves that show decrease of the weight from 29.48% at 3 wt.% glycine to 15.91% at 10 wt.% glycine. Change of heat flow also indicates improvement of chemical interaction with increase in glycine fraction due to the absorption of endothermic energy.

The ZFC and FC curves for yttrium ferrite before and after annealing at 1000 °C, show that the sample containing 3 wt.% glycine has the smallest particle size. The difference of the temperatures T_b and T_i are significantly different, which can be connected with a broad particle size distribution. Magnetization curves for $Y_3Fe_5O_{12}$ samples indicated that at 5 K yttrium ferrite exhibits ferromagnetic behavior while at 300 K it is paramagnetic. Annealing $Y_3Fe_5O_{12}$ samples resulted in an obvious change of the domain structure illustrated by the rectangular hysteresis loop. Obtained rectangular hysteresis loop of $Y_3Fe_5O_{12}$ can be useful in high frequency applications.

Acknowledgment

We acknowledge the financial support of this research by the National Science Foundation Grants 0933140 and HRD-1242090.

References

1. A. Sztaniszlav, E. Sterk, L. Fetter, M. Farkas-Jahnke, J. Laba´r, J. Magn. Magn. Mater. 41 (1-3) (1984) 75-78.
2. M.I. Yanovskaya, T.V. Rogova, S.A. Ivanov, N.V. Kolganova, N.Ya. Turova, J. Mater. Sci. Lett. 6 (3) (1987) 274-276.
3. M. Shang, C. Zhang, T. Zhang, L. Yuan, L. Ge, H. Yuan, and S. Feng, Appl. Phys. Lett. 102, 062903, 2013.
4. M. Leoni, V. Buscaglia, G. Battilana, P. Nanni, G. Randi, Mater. Eng. 3, 105, 1992.
5. S. Nakayama, J. Mater. Sci. 36 (23) (2001) 5643-5648.
6. N. Pandya, P.G. Kulkanrni, P.H. Parsania, Mater. Res. Bull. 25 (8) (1990) 1073-1077.
7. D.S. Todorovsky, R.V. Todorovska, St. Groudeva-Zotova, Mater. Lett. 55 (1-2) (2002) 41-55.
8. M. Inoue, T. Nishikawa, T. Nakamura, T. Inui, J. Am. Ceram. Soc. 80 (8) (1997) 2157-2160.
9. M. Sivakumar, A. Gedanken, W. Zhong, Y.H. Jiang, Y.W. Du, I. Brukental, D. Bhattacharya, Y. Yeshurun, I. Nowik, J. Mater. Chem. 14 (2004) 764-769.
10. K. Suresh, N.R S. Kumar, K.C. Patil, Advanced Materials, 3 (3) (1991) 148-150.
11. K.S. Martirosyan, P.B. Avakyan and M.D. Nersesyan, Inorgan. Mater, 38 (4) (2002) 489-492.
12. J.J. Kingsley, K. Suresh and K.C. Patil, J. Mater. Sci., 25 (2) (1990) 1305-1312.
13. S.T. Aruna, A.S. Mukasyan, Solid State Material Science, 12 (2008) 44-50.
14. K.S. Martirosyan and D. Luss, Chem. Eng. Technology, 32 (9) (2009) 1376-1383.
15. Cullity B.D. Elements of X-ray diffraction (Addison-Wesly Publishing Co. Inc.), 1976.

Received 24 September 2013